SPECIAL TOPIC — A 40th Anniversary Celebration: Physics Research and Innovation at Ningbo University

Superconductivity in ternary yttrium–zirconium hydride under high pressure

Qinghong Gu(谷庆红)[1], Xindeng Lv(吕心邓)[1], Yu Huang(黄宇)[1], Weihao Jia(贾维豪)[1], Dawei He(何大为)[1], Kaiping Hu(胡开平)[1], Xingbin Zhao(赵行斌)[1], Jie Fu(付洁)[1], Yanping Huang(黄艳萍)[1,†], and Tian Cui(崔田)[1,2,‡]

[1] *Institute of High Pressure Physics, School of Physical Science and Technology, Ningbo University, Ningbo* 315211, *China*
[2] *State Key Laboratory of High Pressure and Superhard Materials, College of Physics, Jilin University, Changchun* 130012, *China*

(Received 24 January 2026; revised manuscript received 11 March 2026; accepted manuscript online 13 March 2026)

Compared to binary hydrides, ternary polyhydrides increase the configurational degrees of freedom and offer a richer variety of candidate structures. This significantly expands the search space for high-temperature superconductivity. According to theoretical predictions, *P*4/*mmm*-$YZrH_8$ is a promising superconductor that will exhibit a superconducting transition temperature (T_c) of approximately 60–70 K at 200 GPa. In this work, we successfully synthesized *P*4/*mmm*-$YZrH_8$ under pressures remarkably lower than those used in theoretical calculations. *P*4/*mmm*-$YZrH_8$ shows a T_c ranging from 64 K to 87 K within 167–190 GPa. Besides, the T_c of *P*4/*mmm*-$YZrH_8$ increases at a rate of approximately 1.01 K/GPa, as pressure decreases from 190 GPa. The maximum T_c observed is 87 K at 167 GPa. The upper critical field ($\mu_0 H_{c2}(0)$) at 183 GPa is determined to be 19.3 T (WHH) and 15.7 T (GL), respectively. Moreover, the existence of d-electrons in Zr suppresses the hydrogen-dominated superconductivity of hydrides, thereby leading to a lower T_c. Zr is not an ideal element in ternary yttrium hydrides. Nevertheless, our research provides valuable insights for the future exploration of ternary hydride systems.

Keywords: hydride, superconductivity, high pressure

PACS: 74.25.–q, 07.35.+k, 88.30.rd

DOI: 10.1088/1674-1056/ae5171 **CSTR:** 32038.14.CPB.ae5171

1. Introduction

The study of high-temperature superconductors has remained at the forefront of condensed matter physics and materials science. According to the Bardeen–Cooper–Schrieffer theory,[1] metallic hydrogen was predicted to be a potential high-temperature superconductor due to its high Debye temperature and strong electron-phonon coupling.[2] However, theoretical calculations indicated that the metallization of hydrogen would occur only at extremely high pressures exceeding 500 GPa,[3–5] a condition that has long been difficult to achieve in the experiment. Ashcroft proposed the concept of "chemical precompression",[6] which argued that metal atoms significantly lowered the pressure required for hydrogen metallization, bringing it within experimentally accessible ranges. Thus, superhydrides were considered strong candidates for high-temperature superconductors. Theoretical studies predicted that the covalent hydride H_3S could be a high-T_c superconductor;[7,8] these predictions were experimentally confirmed with the observation of superconductivity at 203 K at 150 GPa.[9]

Following the discovery of high-temperature superconductivity in H_3S, the clathrate hydride LaH_{10} was first synthesized under high pressure and exhibited a T_c near room temperature.[10–13] Inspired by the studies of H_3S and LaH_{10}, significant research has focused on similar structures.[14,15] These predictions have been subsequently confirmed through experimental synthesis. A series of superhydrides have been successfully synthesized, including CaH_6,[16,17] CeH_9,[18–20] and CeH_{10}.[18]

Yttrium hydrides have attracted considerable attention. Experimental studies have confirmed the superconductivity of yttrium hydrides across various stoichiometries, including *I*4/*mmm*-YH_4,[21] *Im*$\bar{3}$*m*-YH_6,[22] and *P*6$_3$/*mmc*-YH_9.[23] Building upon these binary yttrium hydrides, ternary yttrium hydrides incorporating additional elements have been shown to be a highly promising approach. For example, *I*4/*mmm*-(La, Y)H_4 exhibited a T_c of 92 K at 110 GPa.[24] *P*6$_3$/*mmc*-(Y, Ce)H_9 exhibited a T_c ranging from 97 K to 114 K over a broad pressure interval of 98–200 GPa.[25] *Im*$\bar{3}$*m*-(Y, S)H_6 exhibited an exceptionally high T_c of up to 235 K.[26] The *Im*$\bar{3}$*m*-(Y, Ca)H_6 achieved a T_c of approximately 224 K at 155 GPa.[27] The demonstration of superior superconductivity in these ternary hydrides has been accomplished by introducing a third element. Although researchers have conducted numerous studies, the exploration of superconducting properties in ternary hydrides remains promising.

†Corresponding author. E-mail: huangyanping@nbu.edu.cn
‡Corresponding author. E-mail: cuitian@nbu.edu.cn

© 2026 Chinese Physical Society and IOP Publishing Ltd. All rights, including for text and data mining, AI training, and similar technologies, are reserved.

CPB Online In-Press

Recently, extensive theoretical calculations have been performed on the Y–Zr–H system.[28,29] Zhao *et al.*[28] investigated Y-Zr polyhydrides with various stoichiometries, among which $YZrH_8$ has drawn significant attention due to its promising superconductivity. In $YZrH_8$, hydrogen atoms form an H_{18} cage with weak covalent H-H bonds. It was predicted to exhibit a T_c of approximately 60–70 K at 200 GPa.[28] Similar results have been confirmed in the work of Li *et al.*[29] Moreover, given the similar electronegativity of Y and Zr, the Y–Zr–H system is anticipated to yield a distinct structure and superconducting properties under high pressure.[29]

In this work, we focus on the superconducting properties of the ternary Y–Zr–H system. Through five independent experiments, we have successfully synthesized *P*4/*mmm*-$YZrH_8$. Low-temperature electrical transport measurements reveal that its T_c ranges from 64 K to 87 K over the pressure interval of 167–190 GPa. Our study indicates that zirconium may not be a promising third element for enhancing high-temperature superconductivity in ternary yttrium hydrides. Nevertheless, our results provide valuable experience for exploring the superconducting properties of other hydrides.[14]

2. Experimental methods

2.1. Sample synthesis

We used commercially available Y (Beijing Hawk, 99.9%) and Zr (Thermo Scientific, 99.6%) powders to prepare Y–Zr alloys at a Y:Zr molar ratio of 1:1. We first thoroughly mixed the powder mixtures by grinding them in an agate mortar for 3 hours. The powders were then pressed into wafers measuring 4 mm in diameter and 2.5 mm in height. Finally, the wafers were sintered at 5 GPa and 2000 °C for 40 minutes in a cubic anvil high-pressure system (SPD-6 × 14400 kN, Guilin Guiye Heavy Industry Co., Ltd., China). To confirm the homogeneity and determine the elemental composition of the alloys, all samples were characterized using a Regulus 8100 scanning electron microscope equipped with energy-dispersive x-ray spectroscopy (SEM-EDS, Regulus, Hitachi High-Tech Corporation), as shown in Fig. S1 and Table S1. Hydrides were synthesized using a series of diamond anvil cells (DACs), which were fabricated with diamonds featuring 50–60 μm culets. Ammonia borane (NH_3BH_3, 99% purity, Beijing Psaitong Biotechnology Co., Ltd.) was selected as the hydrogen source due to its ability to release hydrogen via thermal decomposition. After compression to the target pressure, laser heating was conducted using an yttrium aluminum garnet (YAG) laser, with the heating temperature ranging from 1500 K to 2000 K.

2.2. Electrical transport measurements

Electronic transport measurements under external magnetic fields were performed in a multifunctional measurement system using a Cu-Be alloy diamond anvil cell (DAC). The system was equipped with a 1.7–300 K cryostat (PHISKE Research Company Inc.) and a 14 T superconducting magnet (Cryomagnetic Inc.). A four-electrode configuration was created by attaching four Pt wires with silver epoxy to the Y–Zr alloy and NH_3BH_3 in the sample chamber, enabling in-plane resistance measurements at high pressures via the Van der Pauw method,[30] as shown in Fig. 1(a). The sample chamber was formed by a tungsten gasket lined with a composite insulating layer composed of boron nitride powder and an epoxy binder.

2.3. X-ray diffraction measurements

X-ray diffraction (XRD) measurements of the samples in DACs were performed at the BL15U1 beamline of the Shanghai Synchrotron Radiation Facility (SSRF), with a wavelength of 0.6199 Å. The collected XRD patterns were integrated and processed using the Dioptas software package,[31] and then analyzed by Le Bail refinement[32] with the GSAS-II package.[33] In all experiments, the pressure was determined by calibrating the Raman shift of the stressed edge of the diamond peak.[34,35]

3. Results and discussion

3.1. Superconductivity in the Y–Zr–H system

To investigate the superconductivity of the Y–Zr–H system, we prepared five DACs for laser heating within the range of 167–190 GPa (Cells 1–5, Table S1). To confirm the synthesis of the Y–Zr–H phase after laser heating, we conducted low-temperature electrical transport measurements both before and after the laser heating. As illustrated in Fig. 1(b), the resistance of the pristine alloy decreased with decreasing temperature and showed a superconducting transition at 11.5 K before laser heating at 176 GPa. Notably, after laser heating, the resistance dropped sharply at 76 K at 182 GPa, suggesting a potential superconducting transition, and reached zero resistance at lower temperatures. We employed the intersection of the two dashed lines in the normal and superconducting states (inset of Fig. 1) to precisely locate the transition temperature. Furthermore, we varied the combinations of current and voltage to measure the *R*–*T* curves (Fig. S2). The two curves with different electrode configurations both exhibited comparable T_c at around 75 K. Additionally, a similar drop in resistance was observed in Cell 2, which exhibited a T_c of 75 K at 178 GPa (Fig. S3), further confirming the reproducibility of superconductivity in our experiments. The superconducting transitions in all five experiments exhibited slight broadening. Because the laser spot size is smaller than the sample size, combined with the extremely high-pressure conditions, this often leads to temperature gradients during the laser heating process. This leads to spatial inhomogeneity and the presence of impurities.

CPB Online In Press

This spatial inhomogeneity is crucial for high-pressure electrical transport measurements, resulting in complex features such as a multistep or broadened superconducting transition observed macroscopically.

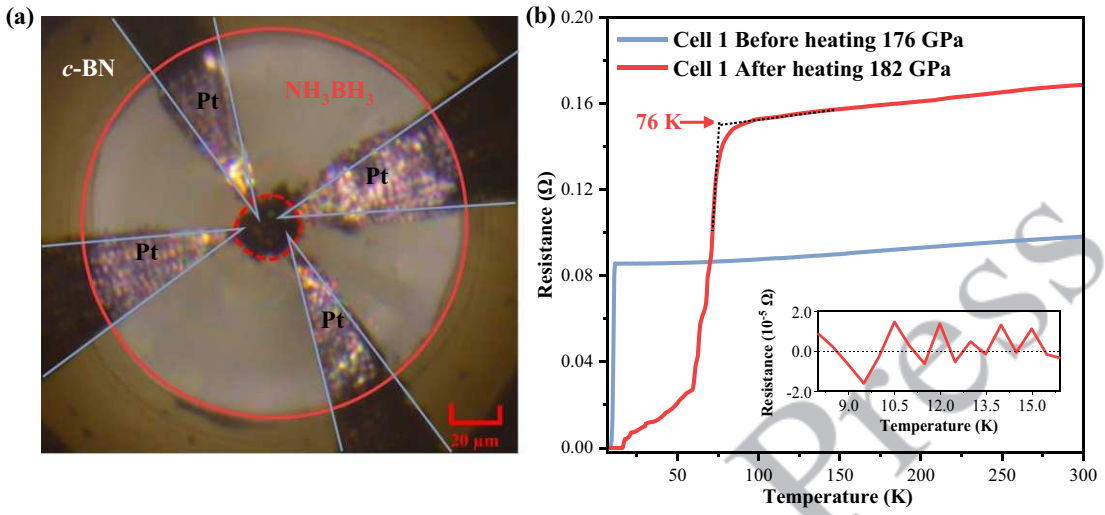


Fig. 1. (a) Image of the high-pressure assembly of the DAC. (b) Temperature dependence of the electrical resistance in Cell 1 before and after laser heating. The inset shows the zero resistance at low temperature.

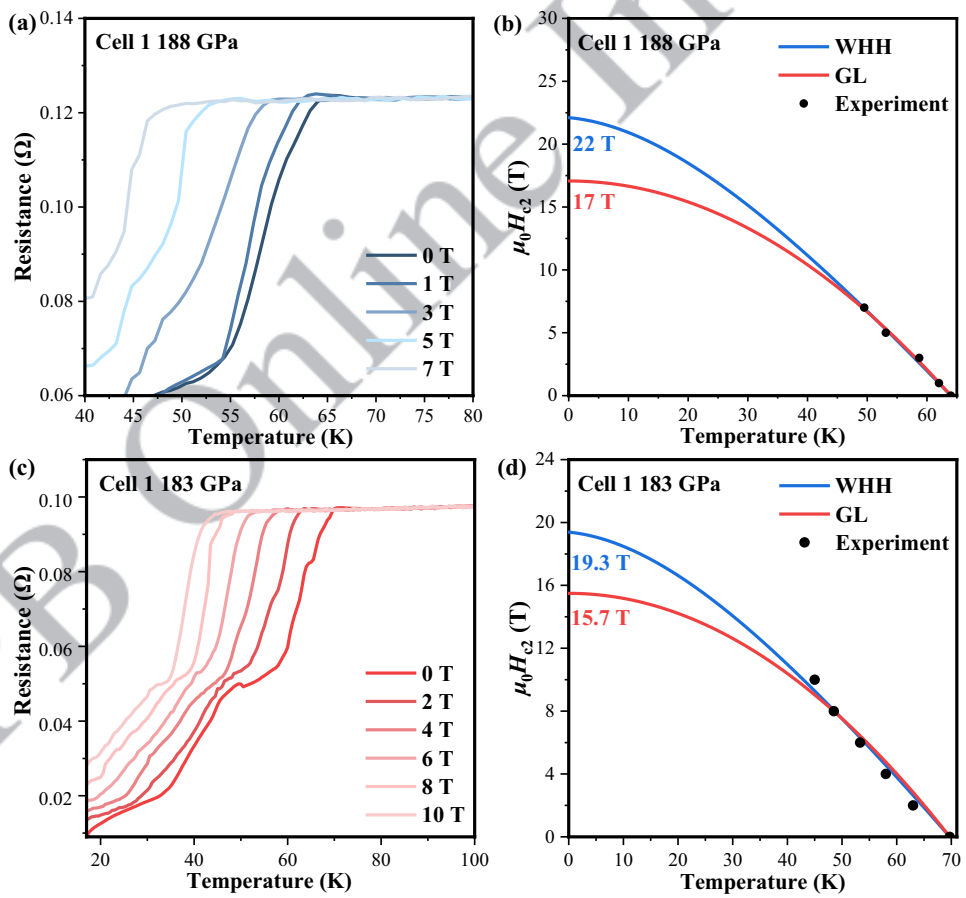


Fig. 2. Electrical resistance measurements of the superconducting transition in external magnetic fields. (a) and (c) Temperature dependence of the resistance in an external magnetic field for Cell 1 at different pressures. (b) and (d) Extrapolated upper critical magnetic fields of Cell 1 for *P*4/*mmm*-$YZrH_8$, fitted using the GL and simplified WHH models. The T_c values are determined using the criterion of T_c^{onset} for the normal-state resistance.

Due to the limited sample dimensions, direct detection of the Meissner effect is challenging under high pressure. Therefore, the suppression of the T_c under an external magnetic field is employed to verify the superconducting phase in the Y–Zr–H system. As shown in Figs. 2(a) and 2(c), the resistance drops shift to lower temperatures as the magnetic field increases from 0 to 10 T for the sample in Cell 1 at different pressures. These behaviors further confirm that the observed resistance

CPB Online In-Press

decrease originated from a superconducting transition. The temperature dependence of the upper critical field, $\mu_0 H_{c2}(T)$, is shown in Figs. 2(a) and 2(c). To estimate $\mu_0 H_{c2}(0)$, we plotted the dependence of T_c on the external magnetic field, as shown in Figs. 2(b) and 2(d). The data are fitted using the Werthamer–Helfand–Hohenberg (WHH)[36] model

$$\mu_0 H_{c2}(T) = \frac{\mu_0 H_{c2}(0)}{0.693}\left[\left(1-\frac{T}{T_c}\right) - 0.153\left(1-\frac{T}{T_c}\right)^2 - 0.152\left(1-\frac{T}{T_c}\right)^4\right], \quad (1)$$

and Ginzburg–Landau (GL)[37,38] models

$$H_{c2} = H_{c2}(0)\left[1-\left(\frac{T}{T_c}\right)^2\right]. \quad (2)$$

The extrapolated $\mu_0 H_{c2}(0)$ at 188 GPa was determined to be approximately 22 T and 17 T, respectively, as shown in Fig. 2(b). In addition, the superconducting coherence length ξ has also been estimated through the formula $\xi = [h/(4\Pi e H_{c2})]^{1/2}$, incorporating the $\mu_0 H_{c2}(0)$ values obtained from the GL and WHH models. The calculated ξ was 3.87 nm from the WHH model and 4.4 nm from the GL model. With the pressure decreasing to 183 GPa, the $\mu_0 H_{c2}(0)$ produced by these two models is 19.3 T (WHH) and 15.7 T (GL), respectively, as shown in Fig. 2(d). Furthermore, the $\mu_0 H_{c2}(0)$ of Y–Zr–H was approximately 3 T lower than that of *I4/mmm*-YH_4 at 179 GPa, with $\mu_0 H_{c2}^{WHH}(0) = 22.2$ T and $\mu_0 H_{c2}^{GL}(0\ \mathrm{K}) = 17.6$ T.[21] Taking the superconducting upper critical field fitted at 183 GPa as an example, we also calculated the coherence length using the above models. The calculation results showed that the coherence length $\xi^{WHH}(0)$ of the superconductor was 4.13 nm according to the WHH model, while the coherence length $\xi^{GL}(0)$ was 4.58 nm. Based on BCS theory,[1] using the formula $\xi(0) = 0.18\hbar v_F/(k_B T_c)$, the Fermi velocity was estimated to be 2.1×10^5 m/s at 183 GPa. We calculated the carrier density from the relationship $n = [1/(3\pi^2)][m_e v_F/\hbar]^3$, and the carrier density was about 2.02×10^{26} m^{-3}. Thus, the London penetration depth was 374 nm using the formula $\lambda(0) = [m_e/(\mu n e^2)]^{1/2}$. The coherence length indicates that the superconducting phase is a typical type-II superconductor.

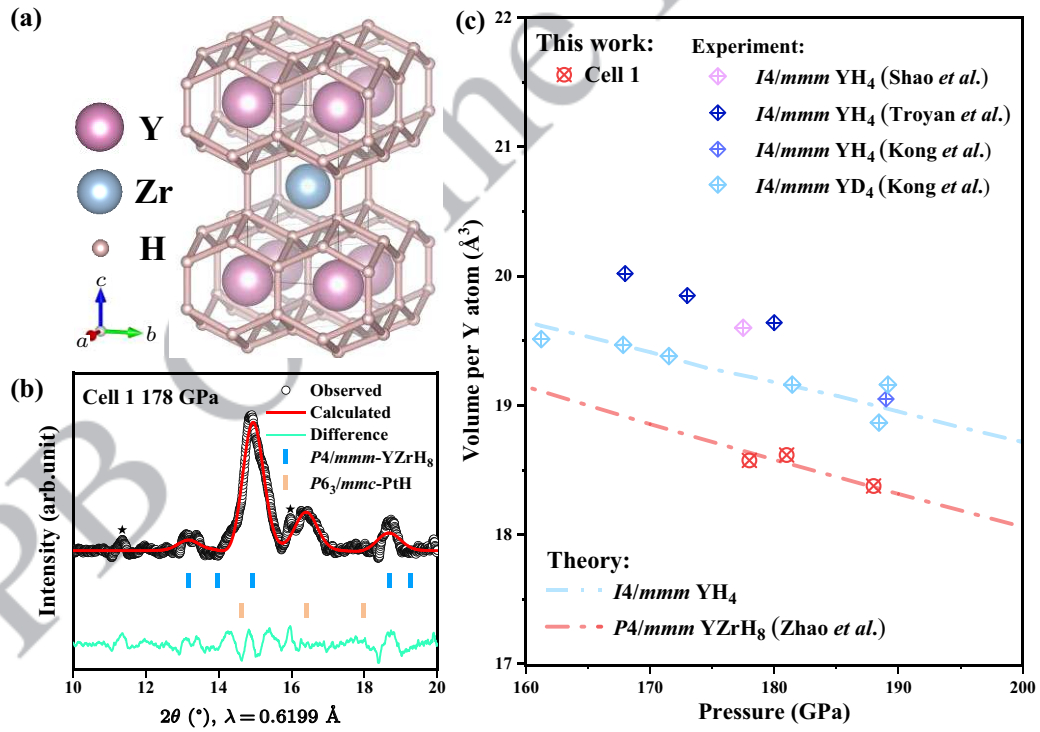


Fig. 3. Structural information for the synthesized *P4/mmm*-$YZrH_8$ at 178 GPa. (a) Crystal structure of *P4/mmm*-$YZrH_8$ at 178 GPa. (b) Le Bail refinement of XRD patterns for *P4/mmm*-$YZrH_8$ at 178 GPa ($\lambda = 0.6199$ Å) in Cell 1. The pentagram denotes an unidentified impurity peak. (c) Volume of the synthesized *P4/mmm*-$YZrH_8$ as a function of pressure. Red solid spheres show the experimental data for *P4/mmm*-$YZrH_8$ in this work. Dark blue, blue, and pink hollow symbols correspond to theoretical and experimental data from previous literature studies.[21–23]

3.2. Structure characterizations

In situ synchrotron XRD measurements were employed to determine the crystal structure of the synthesized sample. For Cell 1, we conducted the XRD measurements under different pressures at room temperature. Our results demonstrated that the XRD patterns revealed minor impurity peaks indexed to *P6*$_3$*/mmc*-PtH.[39,40] The diffraction patterns obtained at 178 GPa for Cell 1 were indexed with the tetragonal *P4/mmm* space group, and the corresponding Le Bail refinement results were presented in Fig. 3(b). We also mea-

CPB Online In-Press

sured the XRD data in Cell 1 at 180 and 188 GPa, as shown in Figs. S4–S5. Given the low x-ray scattering cross section of hydrogen atoms, their positions could not be directly determined from synchrotron XRD patterns. Consequently, the hydrogen stoichiometry (x) could be estimated by the following formula. The value of x was calculated using the formula $x = [(V_{\text{lattice}} - V_{\text{Y}} - V_{\text{Zr}})/V_{\text{H}}]/2$, where V_{lattice}, V_{Y}, V_{Zr}, and V_{H} are the unit cell volume and the volumes of yttrium, zirconium, and hydrogen atoms, respectively. The values of V_{Y}, V_{Zr}, and V_{H} were estimated from the pressure-dependent volume relations of their respective elemental phases, as shown in Fig. S6.[25,41–43] Thus, the experimental hydrogen content was determined to be ~ 8 via formula calculation, consistent with the strategy adopted in previous experiments.[25,44] The calculated hydrogen stoichiometry deviates slightly from the ideal value of 8 due to the direct use of elemental phases for volume evaluation. At the same time, given the experimental difficulties and challenges, a slight discrepancy exists between the XRD diffraction peaks and the theoretical structure. However, the experimentally obtained volume evolution under pressure was compared with the theoretically predicted volume of the Y–Zr–H structure, revealing good agreement between the experimental and theoretical results (Fig. 3(c)).[28] In summary, based on the above results, we successfully synthesized *P*4/*mmm*-$YZrH_8$. In *P*4/*mmm*-$YZrH_8$, hydrogen atoms form H_{18} cages that surround the metal atoms in Fig. 3(a). Furthermore, the cell volume of *P*4/*mmm*-$YZrH_8$ was slightly smaller than that of the binary *I*4/*mmm*-YH_4,[21] and this contraction can be attributed to the partial substitution of Y atoms by smaller Zr atoms.

3.3. The pressure dependence of T_c

To comparatively analyze the pressure dependence of T_c across *P*4/*mmm*-$YZrH_8$, the binary Y–H[21,45] system, and the Zr–H system,[46,47] the evolution of T_c with pressure for these hydrides was summarized in Fig. 4. The complete pressure-dependent datasets for all cells are available in Figs. S7–S9. Electrical transport measurements revealed that within the pressure range of 167–190 GPa, the T_c of these samples exhibited an overall increasing trend with decreasing pressure. The T_c of *P*4/*mmm*-$YZrH_8$ increases at a rate of approximately 1.01 K/GPa, as pressure decreases from 190 GPa. Therefore, *P*4/*mmm*-$YZrH_8$ reaches its maximum T_c of 87 K at 167 GPa, with a minimum T_c of 64 K at 190 GPa. In previous work, the T_c of *I*4/*mmm*-YH_4 remained remarkably stable over the pressure range of 143–180 GPa,[21,45] and *I*4/*mmm*-ZrH_4 was predicted to exhibit a T_c of 47 K at 240 GPa.[46] Compared to the reported *I*4/*mmm*-YH_4,[21,45] the *P*4/*mmm*-$YZrH_8$ exhibited a markedly higher pressure dependence of T_c, yet required a far lower synthesis pressure than that theoretically predicted for *I*4/*mmm*-ZrH_4.[46] Additionally, previous calculations have predicted superconducting behavior in the Y–Zr–H system, specifically indicating that *P*4/*mmm*-$YZrH_8$ exhibited superconductivity with a T_c range of 60–70 K at 200 GPa.[28,29] The T_c range was almost consistent with our experimental data, and *P*4/*mmm*-$YZrH_8$ was successfully synthesized at a pressure remarkably lower than that theoretically predicted.

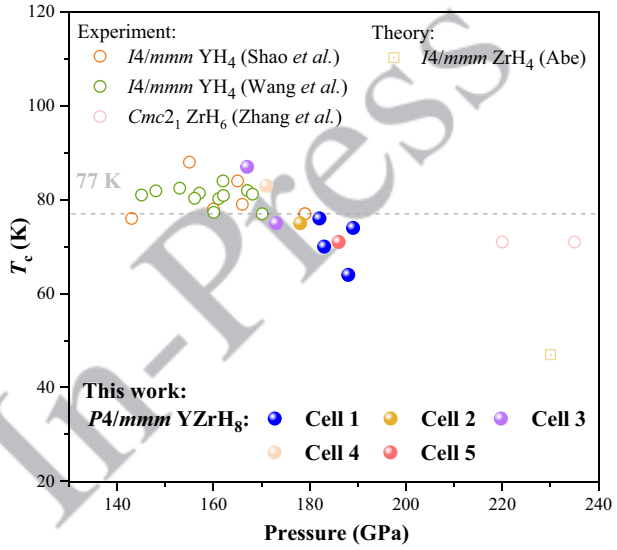


Fig. 4. Pressure dependence of T_c for ternary Y–Zr–H, binary Y–H, and Zr–H systems. Solid spheres show the experimental data for *P*4/*mmm*-$YZrH_8$. Different colors represent different Cells. Orange, green, pink, and brown hollow symbols correspond to the theoretical and experimental data from previous literature studies.[21,45–47]

4. Discussion

In our work, we introduced the element Zr into the Y–H system and successfully synthesized *P*4/*mmm*-$YZrH_8$. Although its T_c shows certain similarities to that of *I*4/*mmm*-YH_4 within the overlapping pressure range, we propose that the two phases are fundamentally distinct, as evidenced by the following aspects: Firstly, within the pressure range of 143–179 GPa, the T_c of YH_4 remains relatively stable, varying from 76 K to 88 K.[21,45] In contrast, the T_c of *P*4/*mmm*-$YZrH_8$ exhibits a marked decreasing trend with increasing pressure from 167 GPa to 190 GPa, as shown in Fig. 4. Secondly, Shao *et al.*[21] reported that YH_4 exhibited a T_c of 76 K at 143 GPa, currently the lowest synthesized pressure for YH_4. In our work, the minimum synthesis pressure for *P*4/*mmm*-$YZrH_8$ can be 167 GPa, and its T_c is 87 K. This indicates that the minimum synthesis pressure required for *P*4/*mmm*-$YZrH_8$ is higher than that for YH_4. Finally, although YH_4 and $YZrH_8$ exhibit similar T_c within their overlapping pressure ranges (Fig. 4), they crystallize in different space groups. XRD characterization further reveals that the unit cell volume of *P*4/*mmm*-$YZrH_8$ is slightly smaller than that of YH_4 under identical pressure conditions, a reduction primarily attributed to the partial substitution of Y atoms by the smaller Zr atoms.

CPB Online In-Press

These pieces of evidence collectively confirm that the synthesized compound is the ternary hydride *P*4/*mmm*-$YZrH_8$ rather than the binary YH_4.

*P*4/*mmm*-$YZrH_8$ exhibits higher synthesis pressures than the binary *I*4/*mmm*-YH_4.[21,45] The underlying reason for the relatively lower superconductivity can be explained from a microscopic perspective. Yttrium (Group IIIB) and zirconium (Group IVB) have similar chemical properties and atomic masses. Although the high-pressure hydrides of yttrium and zirconium all adopt the *I*4/*mmm*-XH_4 (X = Y, Zr) structure, their superconducting properties differ slightly. As metal elements, both Y and Zr atoms can donate electrons to the hydrogen sublattice, which effectively stabilizes the hydrogen framework within the structure. However, they have distinct valence electron configurations: $4s^24p^64d^15s^2$ for Y, $4s^24p^64d^25s^2$ for Zr, and $1s^1$ for H. The zirconium atom has one more d-electron than the yttrium atom, and the presence of this d-electron tends to suppress superconductivity.[29,48] A significant localization of d-electron states near the Fermi level likely suppresses the hydrogen-dominated superconducting mechanism typically operative in such hydrides. This electronic structure feature may account for the relatively lower superconducting performance observed.

The majority of ternary hydrides derived from the *I*4/*mmm*-YH_4 via 50% yttrium substitution exhibited superior superconductivity. For instance, the *I*4/*mmm*-(La, Y)H_4 exhibits enhanced superconducting properties.[24] Its structure remained thermodynamically stable at pressures below 1 megabar. This enhanced low-pressure stability is likely due to configurational disorder introduced by the mixed occupancy La and Y atoms, which plays a crucial role in stabilizing the lattice. Furthermore, extensive theoretical investigations have been conducted on the ternary Y–Sc–H system.[29,49] Calculations predicted that the *P*4/*mmm*-$YScH_8$ was stable at 140 GPa, with a T_c of 110 K. The exceptional superconductivity predicted for the Y–Sc–H system is primarily attributed to two key factors: a high density of states (DOS) derived from hydrogen near the Fermi level and strong electron-phonon coupling.[49] Combining previous research with our study, we have derived an empirical conclusion: isovalent metals enhance T_c, while adjacent element doping reduces superconductivity in ternary yttrium hydrides.

In this work, within the synthesis conditions explored, the *P*4/*mmm*-$YZrH_8$ derived from the Y–Zr alloy enriches the family of ternary Y–Zr–H hydrides. Besides, we hope that our work can provide inspiration for the synthesis of other ternary hydrides, although zirconium does not appear to be a promising third element for enhancing high-temperature superconductivity in ternary yttrium hydrides.

5. Conclusion

In summary, we successfully synthesized the Y–Zr–H compound via laser heating of the Y–Zr alloy with ammonia borane as the hydrogen source, and it was identified as *P*4/*mmm*-$YZrH_8$. The successful synthesis of *P*4/*mmm*-$YZrH_8$ was achieved at pressures below the theoretically predicted value. We present a study of its superconductivity. *P*4/*mmm*-$YZrH_8$ exhibits a T_c ranging from 64 K to 87 K over a pressure range of 167–190 GPa. However, *P*4/*mmm*-$YZrH_8$ exhibited a lower T_c compared to the binary *I*4/*mmm*-YH_4. This phenomenon originates from a substantial localization of Zr d-electrons near the Fermi level, which suppresses the hydrogen-dominated superconducting mechanism and consequently leads to reduced superconductivity. Therefore, under the synthesis conditions explored in this study, zirconium is not an optimal third element for enhancing high-temperature superconductivity in ternary yttrium hydrides. In addition, integrating current references with our work, we have derived an empirical conclusion: isovalent metal incorporation in ternary yttrium hydrides leads to an enhanced T_c, while doping with adjacent elements results in reduced superconductivity.

Acknowledgments

Project supported by the BL15U1 beamline of the Shanghai Synchrotron Radiation Facility (SSRF). This work was supported by the National Key R&D Program of China (Grant Nos. 2023YFA1406200 and 2022YFA1405500) and the National Natural Science Foundation of China (Grant No. 12304072). This work was also supported by the User Experiment Assist System of the Shanghai Synchrotron Radiation Facility (SSRF).

References

[1] Bardeen J, Cooper L N and Schrieffer J R 1957 *Phys. Rev.* **108** 1175
[2] Ashcroft N W 1968 *Phys. Rev. Lett.* **21** 1748
[3] Azadi S, Monserrat B, Foulkes W M C and Needs R J 2014 *Phys. Rev. Lett.* **112** 165501
[4] McMahon J M and Ceperley D M 2012 *Phys. Rev. B* **85** 219902
[5] McMinis J, Clay R C, III, Lee D and Morales M A 2015 *Phys. Rev. Lett.* **114** 105305
[6] Ashcroft N W 2004 *Phys. Rev. Lett.* **92** 187002
[7] Bernstein N, Hellberg C S, Johannes M D, Mazin I I and Mehl M J 2015 *Phys. Rev. B* **91** 060511
[8] Duan D F, Huang X L, Tian F B, Li D, Yu H Y, Liu Y X, Ma Y B, Liu B B and Cui T 2015 *Phys. Rev. B* **91** 180501
[9] Drozdov A P, Eremets M I, Troyan I A, Ksenofontov V and Shylin S I 2015 *Nature* **525** 73
[10] Somayazulu M, Ahart M, Mishra A K, Geballe Z M, Baldini M, Meng Y, Struzhkin V V and Hemley R J 2019 *Phys. Rev. Lett.* **122** 027001
[11] Sun D, Minkov V S, Mozaffari S, Sun Y, Ma Y M, Chariton S, Prakapenka V B, Eremets M I, Balicas L and Balakirev F F 2021 *Nat. Commun.* **12** 6863
[12] Drozdov A P, Kong P P, Minkov V S, Besedin S P, Kuzovnikov M A, Mozaffari S, Balicas L, Balakirev F F, Graf D E, Prakapenka V B, Greenberg E, Knyazev D A, Tkacz M and Eremets M I 2019 *Nature* **569** 528

CPB Online In Press

[13] Geballe Z M, Liu H, Mishra A K, Ahart M, Somayazulu M, Meng Y, Baldini M and Hemley R J 2017 *Angew. Chem. Int. Ed.* **57** 688
[14] Li B, Cao Z S, Zhai J J, Wu M, Chi D, Liu S L and Sun J 2026 *Chin. Phys. Lett.* **43** 010712
[15] Yan X Z, Zhou X Z, Liu C F, Xu Y L, Huang Y B, Sheng X W and Chen Y M 2024 *Chin. Phys. B* **33** 086301
[16] Ma L, Wang K, Xie Y, Yang X, Wang Y Y, Zhou M, Liu H Y, Yu X H, Zhao Y S, Wang H B, Liu G T and Ma Y M 2022 *Phys. Rev. Lett.* **128** 167001
[17] Li Z W, He X, Zhang C L, Wang X C, Zhang S J, Jia Y T, Feng S M, Lu K, Zhao J F, Zhang J, Min B S, Long Y W, Yu R C, Wang L H, Ye M Y, Zhang Z S, Prakapenka V, Chariton S, Ginsberg P A, Bass J, Yuan S H, Liu H Z and Jin C Q 2022 *Nat. Commun.* **13** 2863
[18] Chen W H, Semenok D V, Huang X L, Shu H Y, Li X, Duan D F, Cui T and Oganov A R 2021 *Phys. Rev. Lett.* **127** 117001
[19] Li X, Huang X L, Duan D F, Pickard C J, Zhou D, Xie H, Zhuang Q, Huang Y P, Zhou Q, Liu B B and Cui T 2019 *Nat. Commun.* **10** 3461
[20] Salke N P, Davari Esfahani M M, Zhang Y J, Kruglov I A, Zhou J S, Wang Y G, Greenberg E, Prakapenka V B, Liu J, Oganov A R and Lin J F 2019 *Nat. Commun.* **10** 4453
[21] Shao M Y, Chen W H, Zhang K X, Huang X L and Cui T 2021 *Phys. Rev. B* **104** 174509
[22] Troyan I A, Semenok D V, Kvashnin A G, Sadakov A V, Sobolevskiy O A, Pudalov V M, Ivanova A G, Prakapenka V B, Greenberg E, Gavriliuk A G, Lyubutin I S, Struzhkin V V, Bergara A, Errea I, Bianco R, Calandra M, Mauri F, Monacelli L, Akashi R and Oganov A R 2021 *Adv. Mater.* **33** 2006832
[23] Kong P P, Minkov V S, Kuzovnikov M A, Drozdov A P, Besedin S P, Mozaffari S, Balicas L, Balakirev F F, Prakapenka V B, Chariton S, Knyazev D A, Greenberg E and Eremets M I 2021 *Nat. Commun.* **12** 5075
[24] Bi J K, Yuki N, Zhang P Y, Wang Y Y, Ma L, Wang Y, Bo Z, Katsuya S, Liu H, Zhou M, Wang H B, Liu G T and Ma Y M 2022 *Mater. Today Phys.* **28** 100840
[25] Chen L C, Luo T, Cao Z Y, Dalladay Simpson P, Huang G, Peng D, Zhang L L, Gorelli F A, Zhong G H, Lin H Q and Chen X J 2024 *Nat. Commun.* **15** 1809
[26] Zhang K X, Chen W H, Zhang Y C, Guo J N, Chen S, Huang X L and Cui T 2024 *Sci. China Phys., Mech. Astron.* **67** 238211
[27] Zhang K X, Guo J N, Wang Y L, Wu X Y, Huang X L and Cui T 2025 *Chin. Phys. Lett.* **42** 110704
[28] Zhao W D, Song H, Du M Y, Jiang Q W, Ma T C, Xu M, Duan D F and Cui T 2023 *Phys. Chem. Chem. Phys.* **25** 5237
[29] Li X J, Hao Y Z, Liu Y J, Wang X Y, Lookman T, Sun J, Ding X D and Gao Z B 2025 *J. Chem. Phys.* **163** 104107
[30] Ramadan A A, Gould R D and Ashour A 1994 *Thin Solid Films* **239** 272
[31] Prescher C and Prakapenka V B 2015 *High Pressure Res.* **35** 223
[32] Le Bail A 2012 *Powder Diffr.* **20** 316
[33] Toby B H 2001 *J. Appl. Crystallogr.* **34** 210
[34] Akahama Y and Kawamura H 2006 *J. Appl. Phys.* **100** 043516
[35] Baer B J, Chang M E and Evans W J 2008 *J. Appl. Phys.* **104** 034504
[36] Helfand E and Werthamer N R 1964 *Phys. Rev. Lett.* **13** 686
[37] Ginzburg V L 1955 *Nuovo Cimento* **2** 1234
[38] Baumgartner T, Eisterer M, Weber H W, Flükiger R, Scheuerlein C and Bottura L 2014 *Supercond. Sci. Technol.* **27** 015005
[39] Huang G, Peng D, Luo T, Chen L C, Dalladay Simpson P, Cao Z Y, Gorelli F A, Zhong G H, Lin H Q and Chen X J 2023 *J. Phys.: Condens. Matter* **36** 075702
[40] Matsuoka T, Hishida M, Kuno K, Hirao N, Ohishi Y, Sasaki S, Takahama K and Shimizu K 2019 *Phys. Rev. B* **99** 144511
[41] Anzellini S, Bottin F, Bouchet J and Dewaele A 2020 *Phys. Rev. B* **102** 184105
[42] Samudrala G K, Tsoi G M and Vohra Y K 2012 *J. Phys.: Condens. Matter* **24** 362201
[43] Ji C, Li B, Liu W J, Smith J S, Majumdar A, Luo W, Ahuja R, Shu J F, Wang J Y, Sinogeikin S, Meng Y, Prakapenka V B, Greenberg E, Xu R Q, Huang X R, Yang W G, Shen G Y, Mao W L and Mao H K 2019 *Nature* **573** 558
[44] Bi J K, Nakamoto Y, Zhang P Y, Shimizu K, Zou B, Liu H Y, Zhou M, Liu G T, Wang H B and Ma Y M 2022 *Nat. Commun.* **13** 5962
[45] Wang Y, Wang K, Sun Y, Ma L, Wang Y, Zou B, Liu G, Zhou M and Wang H 2022 *Chin. Phys. B* **31** 106201
[46] Abe K 2018 *Phys. Rev. B* **98** 134103
[47] Zhang C L, He X, Li Z W, Zhang S J, Feng S M, Wang X C, Yu R C and Jin C Q 2022 *Sci. Bull.* **67** 907
[48] Xie H, Zhang W T, Duan D F, Huang X L, Huang Y P, Song H, Feng X L, Yao Y S, Pickard C J and Cui T 2020 *J. Phys. Chem. Lett.* **11** 646
[49] Shi L T, Si J G, Turnbull R, Liang A, Liu P F and Wang B T 2024 *Phys. Rev. B* **109** 054512

CPB Online In Press